Available online at www.sciencedirect.com

jmr&t Journal of Materials Research and Technology

journal homepage: www.elsevier.com/locate/jmrt

Effect of solutionizing and double ageing treatments on the microstructural characteristics and tensile properties of Inconel 718 welds

K. Devendranath Ramkumar [a,*], *A. Vishnu Arvind* [a], *K.V. Rama Aravinth* [a], *E. Srivatson* [a], *Supriyo Ganguly* [b]

[a] *School of Mechanical Engineering, Vellore Institute of Technology, Vellore, 632014, India*
[b] *Welding Engineering & Laser Processing Centre, Cranfield University, Bedford, United Kingdom*

ARTICLE INFO

Article history:
Received 14 June 2023
Accepted 3 September 2023
Available online 7 September 2023

Keywords:
Inconel 718
Laser-arc hybrid welding
Pulsed current gas tungsten arc welding
Ageing treatments
Microstructure characteristics
Tensile properties

ABSTRACT

Inconel 718 joints were fabricated using the pulsating direct current gas tungsten arc welding (PDCGTAW) and laser-arc hybrid welding (LAHW) techniques using Ni-Cr-Mo-rich filler. A cyclic post-weld heat treatment (PWHT) comprising 980 °C/20 min/air cooling; followed by two-stage ageing 720 °C/8 h/furnace cooling and 620 °C/8 h/air cooling was performed on both joints. The liquation cracking was noticed on the heat-affected zone (HAZ) of the LAHW joints. Microstructural characteristics were assessed on the joints in both as-welded (ASW) and PWHT conditions. Regardless of the joints, the coarse Mo-rich segregates were noticed in the fusion zone (FZ) in the ASW conditions. On the contrary, the partial dissolution of MC, precipitation of δ-Ni_3Nb needles and the coarsening of strengthening precipitates were observed on LAHW and PDCGTAW joints after subjecting to cyclic PWHT respectively. Tensile studies corroborated that there is a considerable enhancement in the tensile and 0.2% offset yield strengths of LAHW joints after being exposed to PWHT, despite the formation of HAZ liquation cracking.

1. Introduction

Ni-Fe-Cr-Nb based alloy, Inconel 718 finds use in high-temperature applications in land-based gas turbines and aero-gas turbines, space shuttle rocket engines, fasteners, shafts, and compressors due to its outstanding strength and corrosion resistance. As stated by Niang et al. [1]; this γ″-precipitation strengthened alloy offers excellent resistance to strain age cracking upon PWHT. To achieve optical mechanical strength and corrosion resistance, proper heat treatments are required. Although the alloy imparts excellent weldability, liquation cracking at the fusion zone (FZ), microfissuring at the HAZ, and precipitation of δ-phase and Laves phase are some of the significant issues during the welding Inconel 718 alloy [2]. Documented that the precipitation of Laves phase could be controlled by adopting low welding heat cycles and rapid cooling rates. These authors further recommended the practice of adopting pulsating direct current (PDC) in the GTA welding and Nb-free fillers for lowering the occurrence of Laves phase [3]. Adopted PDCGTA welding to fabricate 5 mm thick plates of Inconel 718 by utilizing Ni-Mo rich, Nb-free fillers. Though, the authors noticed a significant

* Corresponding author.
E-mail address: deva@vit.ac.in (K. Devendranath Ramkumar).
https://doi.org/10.1016/j.jmrt.2023.09.016

reduction in the subsistence of Laves phase. However, the Mo-rich segregates formed in the inter-dendritic regions deteriorated the tensile strength of the joints [4]. Fabricated 5 mm thick joints of Alloy 718 of two different grain sizes ASTM #4 and #10 using CO_2 laser welding. Furthermore, they performed microstructural studies and mechanical integrity of the joints in the as-welded (AW) and PWHT conditions. The researchers observed the micro-fissures at the HAZ while welding Inconel 718 alloy of ASTM #4 and reported that the grain size has a significant influence on the liquation cracking. The authors have also noticed the distribution of deleterious Laves phase and δ-needles in the fusion zone in both conditions [5]. Examined the pulsed Nd: YAG laser welding characteristics of 2 mm thick Inconel 718 sheets. The laser weld joints were then subjected to solution treatment and ageing conditions at different temperatures. Despite the low heat input and slow cooling rates, the inter-dendritic segregation of Laves phase was noticed in the FZ of laser-welded joints. Although the authors performed a solution treatment at 1080 °C to carry out the dissolution of Laves phase, a significant grain coarsening was observed on the base alloy, which, in turn, deteriorated the mechanical properties [6]. Adopted a cyclic post-weld heat treatment involving a solutionizing treatment at 980 °C/1 h/water quenching (WQ) followed by two-step ageing at 720 °C/8 h/furnace cooling (FC) to 620 °C/8 h/air cooling (AC) to room temperature for the hot isostatically pressed Inconel 718. These investigators documented that adopting such cyclic heat treatments considerably improves the tensile properties of Inconel 718 compared to the wrought heat-treated alloy.

Laser-arc hybrid welding (LAHW) receives principal focus in shipbuilding, oil and gas, aerospace, and nuclear industries as the technique offers lower distortion and better gap-bridging ability as noted by Bang et al. [7]. In addition, the combination of arc and laser sources in the weld pool results in deeper penetration welds than traditional laser welds. The use of arc welding consumables such as gas mixtures, offers a high degree of control over the quality of welds and weld properties that is conceivable with autogenous laser welding techniques. Even though Liu et al. [8] have successfully adopted Laser-MIG hybrid welding of 10 mm thick plates of Fe-Co-Ni-based GH909 alloy, the porosity evolved in the weld zone of LAHW lowered the tensile properties of the joints. In another study by Liu et al. [9], the authors observed the porosity and centreline cracks in the fusion region during LAHW of 19 mm thick 17-4 PH grade stainless steel. These authors recommended using Nitrogen as shielding gas in hybrid welding which mitigates the porosity in the FZ [9]. Have successfully adopted LAHW for joining difficult-to-weld martensitic stainless steel grade, AISI 416. The study attests that the joints established through the LAHW process are free from porosity and solidification cracking while following appropriate weld process specifications.

It is opined from the published data that the LAHW technique could be adopted for different alloys. However, the weldability and mechanical traits of LAHW joints of Inconel 718 have not been explored thoroughly. Also, the influence of cyclic post-weld heat treatment of LAHW joints of Inconel 718 has not been systematically assessed. In this research work, the laser - Metal Inert Gas (MIG) hybrid welding is attempted to join 5 mm thick plates of Inconel 718 using a Ni-rich, Nb-free austenitic filler consumable, ERNiCrMo-4. In order to compare the weldability, microstructure transformation, and tensile properties, PDCGTA welding is also used to establish the Inconel 718 joints with the same consumable. Both the LAHW and PDCGTAW joints were then subjected to the cyclic PWHT comprising solutionizing at 980 °C/20 min/AC; followed by two-stage ageing at 720 °C/8 h/FC and to 620 °C/8 h/AC. The microstructural characteristics and tensile behaviour of the joints were examined before and after subjecting to cyclic PWHT.

2. Experimental procedure

2.1. Base alloy and welding processes

The experimental alloy used in the study is hot-rolled Inconel 718 of 5 mm thickness and the chemical composition analysis is presented in Table 1. It was machined using numerically controlled wire-cut electrical discharge machining (WEDM) to extract The rectangular plates of dimensions 250 mm × 55 mm × 5 mm. Standard, single V-groove butt configurations were utilized in the base alloy to carry out the PDC GTA welding process; whereas, square butt configurations were adopted for joining 5 mm thick Inconel 718 plates by the LAHW process.

The filler consumable used for achieving the joints is ERNiCrMo-4 of 1.6 mm diameter. Before welding trials, a grinding wheel was used to remove any oxide scale from the plates, and an acetone solution was used to clean the edges of the plates to remove any contaminations. During LAHW, compressed air was used to protect the focal lens. Argon of high purity (99.9%) was employed as a shielding gas with a flow gas rate of 1.5 m^3/h to shield the weld pool from high-temperature oxidation. A 3.5 kW high-energy, CO_2 laser is used for this study. A MIG welding machine [KEMPII MIG – Pro Evolution 4200 power source] coupled with a wire feeder (Pro MIG 530) was employed together with laser welding to establish hybrid joints. A 10.9 μm wavelength, continuous wave carbon-di-oxide laser beam was focused on the surface of the base alloy by keeping the laser spot diameter at 180 μm and

Table 1 – Chemical composition of base and filler metals.

Base/Filler metal	Chemical Composition (% weight)							
	Ni	Cr	Nb	Mo	C	Fe	Ti	Other elements
Inconel 718	52.29	18.52	5.03	3.3	0.027	Rem.	0.989	P-0.004; Al-0.5; S-0.012; Si-0.1; Mn-0.1; Ta-0.012; Cu –0.07;
ERNiCrMo-4	57.88	15.66	Nil	15.81	0.009	Rem	–	Si-0.055; Mn-0.520; S-0.004; P-0.007; V-0.041; W-3.98; Cu-0.026

the focal length of 300 mm. The feed rate of the filler was kept constant at 6 m/min During the hybrid welding. Both the laser and MIG sources were equipped on a 3-axes FANUC CNC to have a hybrid mode of operation to carry out welding in laser-leading mode. The base alloy plates were fastened firmly in the workbench with the use of U-clevis to provide the welding optics with an accurate inclination to the direction of welding. An appropriate inclination of the optics is required to prevent the splashing metal from prejudicing the lens during the hybrid welding process. A copper backplate with circular grooves was placed to prevent heat convergence in the base alloy. Tack welding was done at both ends of the plates before welding to avoid distortion and misalignment during the welding process. The multi-pass PDC GTA welding process was adopted by fluctuating the currents between 80 and 110 A with a pulsating frequency of 10 Hz. The duty cycle is maintained at 50%. High-purity Argon (99.9%) was used as both the shielding and back-purging gas. The gas flow rates for shielding and back purging were maintained to be 15 and 5 lpm respectively. At the end of every pass, the plates were allowed to reach a temperature of 100 °C, and the plates were cleaned with a stainless steel wire brush. The process specifications adopted for the LAHW and PDC GTAW are provided in Table 2 and Table 3 respectively. Ensued welding, the joints were subjected to a non-destructive examination using X-ray radiography.

Further, the joints established from these welding processes were subjected to a cyclic PWHT comprising solutionizing treatment at 980 °C/20 min/AC; followed by two-stage ageing at 720 °C/8 h/FC and 620 °C/8 h/AC. The samples were cut transversely from the weld joints both in the as-welded and cyclic PWHT conditions to perform a metallurgical examination and integrity tests.

2.2. Microstructure characterization and mechanical integrity tests

Transversely machined samples of measurements 30 mm × 10 mm × 5 mm from these weld joints were used for both the metallographic examination and micro-hardness measurements. Standard metallography practices were adopted to carry out the microstructural characterization. 10% oxalic acid was used to etch the samples electrolytically. Primitive microstructural characterization studies were done using the optical microscope. A detailed characterization of microstructures and the composition of phases were investigated using a field emission scanning electron microscope (FE-SEM) coupled with an energy-dispersive X-ray analyzer (EDS). A Vicker's micro-hardness tester was used to compute the indentation values across the entire width of the transverse samples of both joints with a load of 500 gf, in the ASW and PWHT conditions. Tensile properties were evaluated on the transversely sectioned samples fabricated in accordance with ASTM E23:12C using an Instron UTM [100 kN capacity]. A lower strain rate of $5.5 \times 10^{-4}\ s^{-1}$ was allowed to induce on the gauge length of the joints by providing the cross-head velocity as 1 mm/min. Both the weld joints in the ASW and PWHT conditions were tested in triplicate to determine the average yield and tensile strengths. Also, the base alloy was tested in both conditions for comparative analysis.

Table 3 – Process specifications employed in the Laser-arc hybrid welding of Inconel 718.

Process Parameter	Unit	Value
Laser Power	kW	2.5
Laser mode	–	Continuous Wave
Focal length	mm	300
Travel Speed	mm/min	1000
Shielding gas flow rate	m^3/hr	1.2-1.5
Torch Angle	°	55
MIG Current	A	150
MIG Voltage	V	28.5
Distance between laser and arc	mm	3
Filler Material	–	ERNiCrMo-4
Filler Wire feed rate	m/min.	6
Heat Input	kJ/m	0.1539

3. Results and discussion

3.1. Microstructural characterization

The non-destructive examination evinced that the joints acquired from both LAHW and PDCGTAW are free from porosity, lack of fusion, under-cut and spatter, etc. The transverse macro-graphs of the welded joints shown in Fig. 1(a) and (b) also attest to the absence of any of these defects. The macrostructure of both the joints illustrated that complete intermixing has occurred between the base alloy and consumables used. The hybrid weld joint comprises a wider, upper arc zone (MIG FZ) and a narrower, lower laser zone (Laser FZ) and thus LAHW joints elicited a "wine-glass" shape feature. With the arrangement of the leading laser and trailing MIG (LLTM) approach, the MIG source originates after the laser beam. This, in turn, facilitates the molten metal of filler consumables to expand widely because of the arc forces. The penetration of weld strongly depends on the strength of the key-hole effect as stated by Liu et al. [8]. In the hybrid welding technique, the arcing energy is found to

Table 2 – Process specifications employed in PDC GTA welding of Inconel 718.

Filler wire	Pass	Current (A)		Voltage (V)	Frequency (Hz)	Duty cycle (%)	Heat Input at every pass (kJ/mm)
		I_b	I_p				
ERNiCrMo-4	Cap	80	110	10.1–10.3	10	50	0.738
	Filling pass 1	80	110	10.1–10.5	10	50	0.748
	Root	80	110	10.6–11.5	10	50	0.822

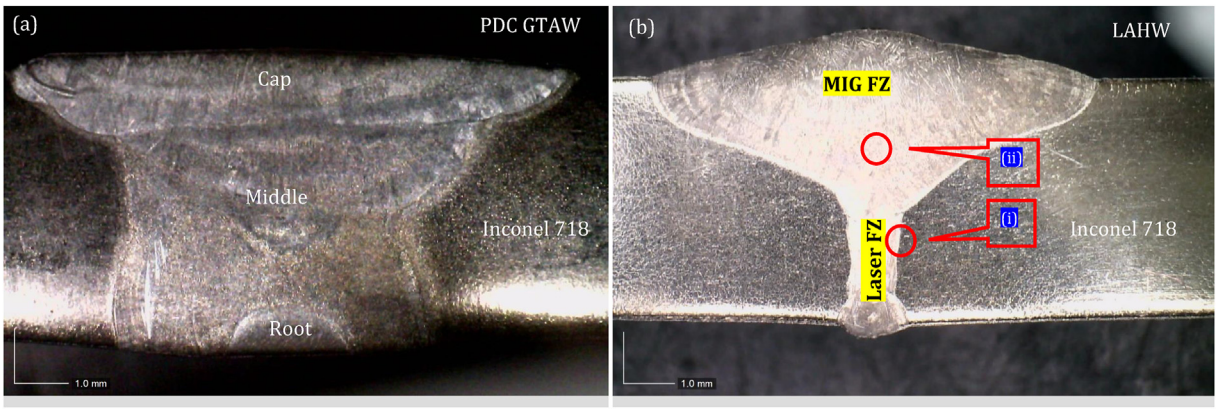

Fig. 1 – Cross-sectional macrographs showing the full penetration joints of Inconel 718 achieved by (a) Pulsed direct current GTA welding and (b) Laser-MIG hybrid welding techniques respectively adopting ERNiCrMo-4 filler.

act predominantly on the top region to impart a wider arc zone. On the contrary, the laser energy impinges on the bottom portion of the sample by the keyhole effect. In the LLTM torch approach, there is a greater possibility of an inward molten globule coercing this keyhole to close, whilst the laser exerts the force in the reverse direction. This facilitates the recirculation of the molten metal at the root region to undergo adequate mixing and aids in generating the laser zone with distinct, greater penetration welding attributes as stated by Muhammed et al. [10]. The base alloy microstructure comprises coarse, Ni-rich γ-grains with the existence of twin boundaries and polygonal-shaped, strengthening (Ti, Nb)C phase as noticed from Fig. 2 in the as-received condition.

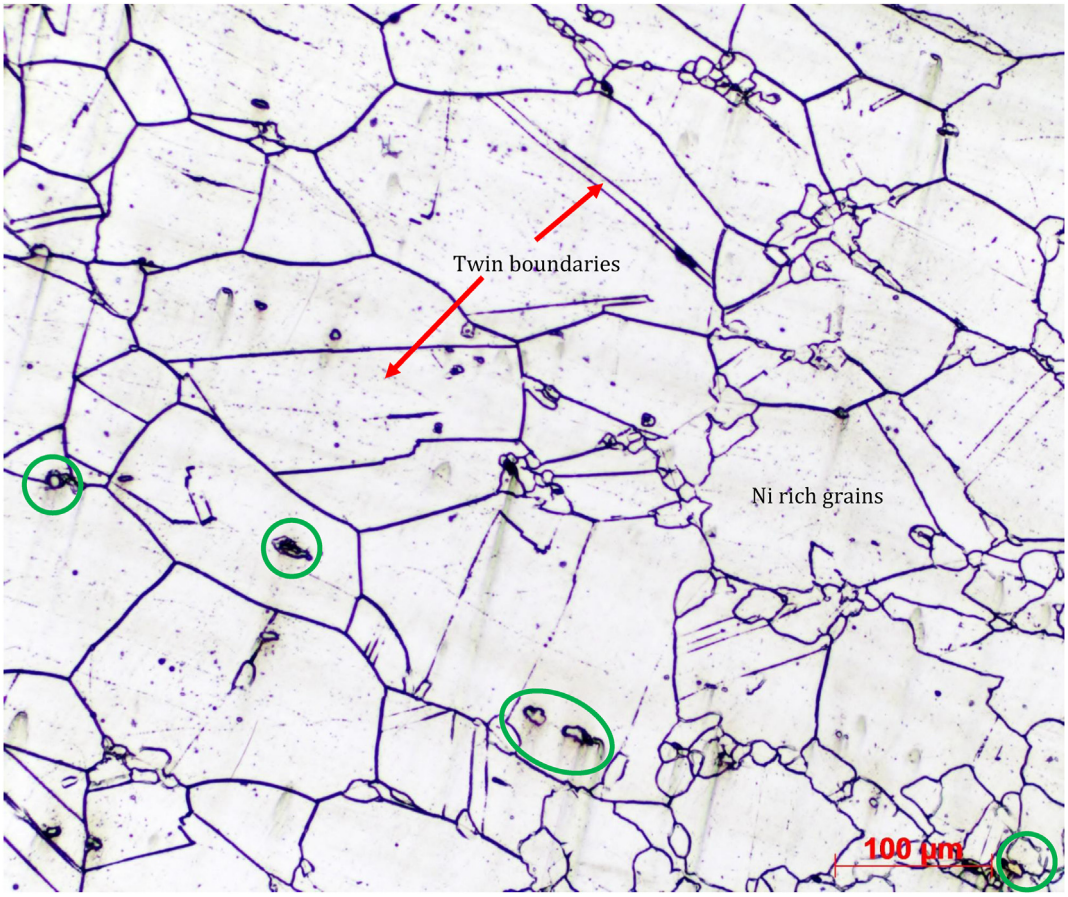

Fig. 2 – Microstructure of the base alloy, Inconel 718 with the twin boundaries and precipitation of (Nb,Ti)C phase.

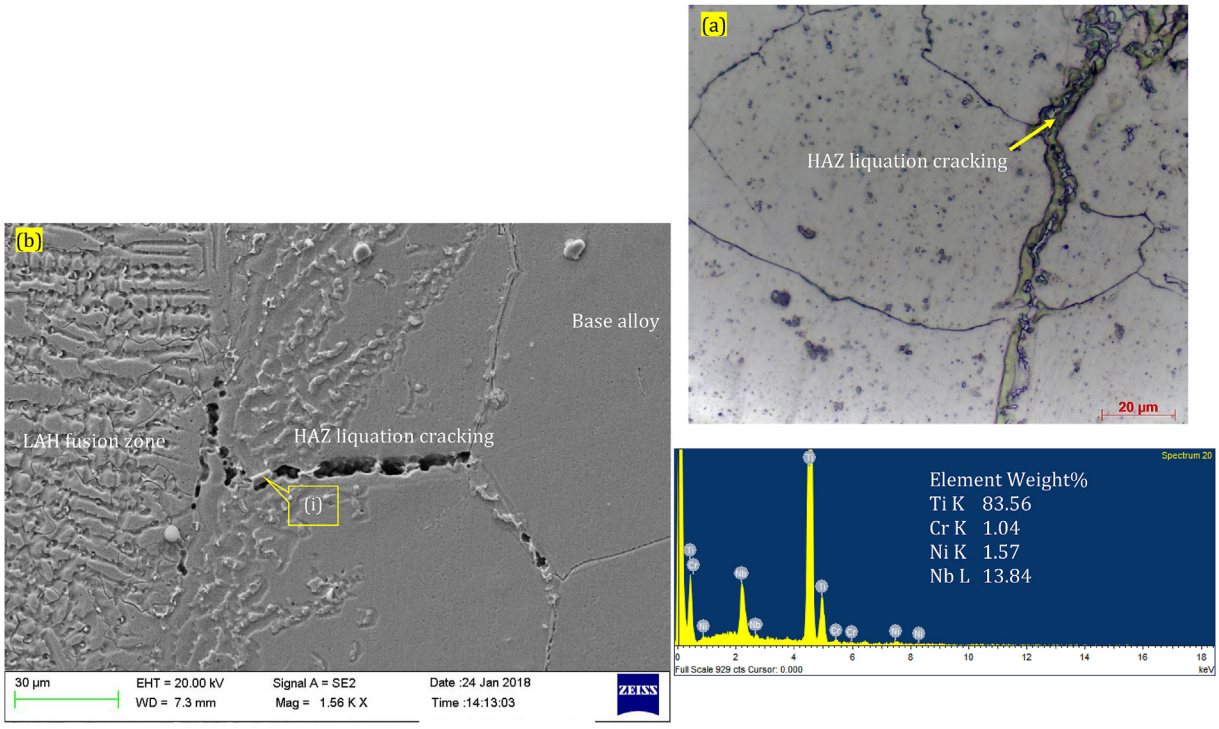

Fig. 3 – Interface microstructure of laser-arc hybrid welded Inconel 718 joints showing the (a) liquation cracking in the HAZ and (b)FE-SEM/EDS analysis on the liquated crack region.

3.1.1. *LAHW joints - as-welded and PWHT conditions*

The interface and weld microstructures of the LAHW joints in the ASW condition are illustrated in Figs. 3 and 4. The occurrence of micro-fissures/liquated grain cracks is noticed in the HAZ of LAHW joints as inferred from Fig. 3(a). The grain size influences the liquation cracking susceptibility. The grain size of the base alloy is #ASTM 5, which is considered to be coarser and hence prone to liquation cracking. The micro-fissuring or liquation cracking at HAZ emanates under the influence of thermally generated stress, which acts as a driving force, causing de-cohesion along with the solid-liquid interfaces at the liquation grain boundary. The low melting eutectic compounds developed in the austenitic grain boundaries are believed to be the reason for the liquation cracking at the HAZ. The constitutional liquation of MC-type carbides favours promoting the susceptibility to HAZ liquation cracking in the Ni-based superalloys. The SEM/EDS analysis results shown in Fig. 3(b) attested to the presence of local liquation of the

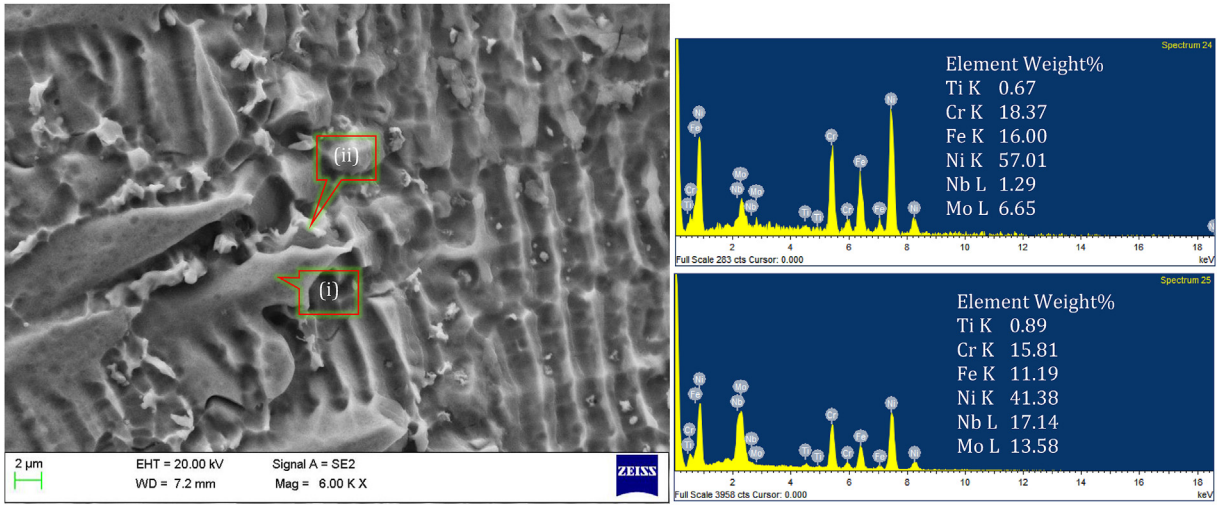

Fig. 4 – Fusion zone microstructure of LAH welded Inconel 718 joints and the EDS analysis at the dendritic and inter-dendritic regions in the as-welded conditions.

intermetallic compound, TiC on the liquated, jagged crack region [Zone (i) indicated in Fig. 1(b)]. In a study, Radavich [11] also concluded that TiC plays a significant role in HAZ liquation cracking. The author stated that the films of grain boundary carbides crystallize and either force the grains to isolate or separate them embrittled and vulnerable to cracking under stresses induced during welding. Moreover, the heating and cooling cycles in the laser-arc hybrid welding process are non-equilibrium and also very high. Hence, the MC-type carbides do not have the possibility to dissolve in the matrix of Ni-based superalloy. This non-equilibrium, sub-solidus melting of secondary phases such as TiC, NbC, and other MC carbides is known to cause liquation cracking. The microstructure is another major factor that greatly affects the propensity to HAZ liquation cracking. The grain size was found to be coarsened in the HAZ closer to the FZ boundary line. According to Yan et al. [12], the zigzag grain boundary imparts higher resistance to cracking due to the enhanced bonding characteristics between the adjoining crystals and delays the initiation and propagation of the crack. In contrast, the propensity of expanding the liquation cracks is high in the straight grain boundary because of the limited resistance to cracking. The FZ microstructure comprises both the columnar dendritic grains along the fusion boundary line and fine equiaxed dendritic grains in the centreline in the upper seam of the LAHW joints. Whereas the bottom and central regions predominantly have columnar dendritic structures. Secondary dendrites also originated from the columnar crystals as seen in Fig. 4 [Zone (ii) indicated in Fig. 1(b)]. Inter-dendritic segregation of secondary phases richer in Nb-Mo content is revealed clearly from the SEM analysis shown in Fig. 4 and also the existence of compositional mismatch in the dendritic and inter-dendritic regions. The composition of the elements Ni, Nb and Mo content in the inter-dendritic and dendritic regions are significantly varying. The SEM analysis of the LAHW joints of Inconel 718 in the PWHT conditions attested that the variations in the composition of the elements in the dendritic and inter-dendritic regions become significantly lowered. Further, it is opined from the microstructure that the weld matrix has not undergone any changes in the grain size indicating that grain growth is inhibited. Also, as the ageing temperature is increased, the strengthening precipitates and MC carbides coarsened gradually along the grain boundaries as seen in Fig. 5. The observations are consistent with the previous reports of An et al. [13]. The study also attests to the non-occurrence of Laves phase in the fusion zone of Alloy 718 joints obtained from the LAHW technique.

3.1.2. *PDCGTAW joints*

The heat-affected zone of Inconel 718 joints obtained from the PDCGTAW process resulted in finer grains due to the pulsation in the current flow as shown in Fig. 6. The optical microscopy image indicated the prominent regions of HAZ, base metal, and the fusion zone of multi-pass PDCGTA welded Inconel 718. The dispersion of (Ti, Nb)CN precipitates is noticed in the HAZs of Inconel 718. A controlled heat input developed in the PDCGTA welding process resulted in a finer grain size than that of the base alloy which is evident from Fig. 6. Also, the partially melted zone (PMZ) is observed adjacent to the FZ. The base alloy just next to the FZ usually undergoes a degree of peak temperatures i.e. between the liquidus and non-equilibrium solidus temperature of the alloy, during multi-pass welding. Hence, the microstructure formed in this region will endure partial melting and a PMZ occurs. Several investigators reported the occurrence of liquation cracking in the PMZ in various superalloys. However, the authors didn't observe any liquation cracks in the HAZ in the current studies. Also, a fine-grained HAZ is noticed alongside the PMZ. During welding, grain growth and recrystallization are the two major microstructural changes encountered in welding Ni-based alloys. In the fine-grained HAZ, the growth of grains is less pronounced due to the segregation in grain boundaries.

The FZ microstructure of multi-pass PDCGTAW joints contains both equiaxed and columnar grains in the form of weld packets. During the process of weld metal solidification, the dendrites grow in the direction of the weld centre from the fusion boundary. In the case of the pulsed direct current GTAW process, the weld pool disengages the tip of the expanding dendrite in advance of the solidification front as a result of the alteration of the arc intensity. Hence, the dendrites get fragmented, acting as heterogeneous sites of

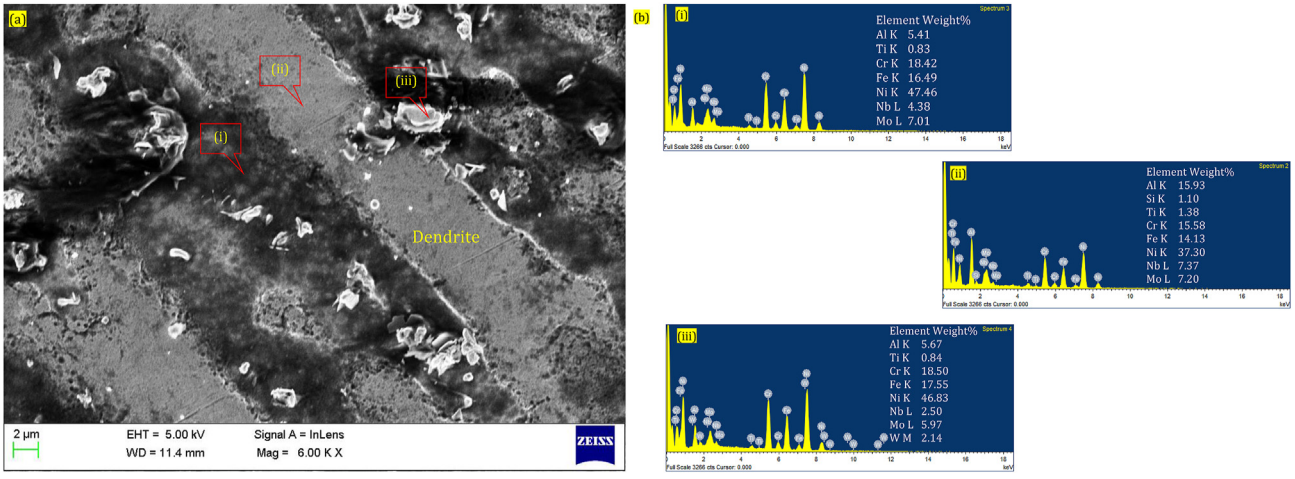

Fig. 5 – (a) FE-SEM image showing the fusion zone microstructure of LAHW joints of Inconel 718 in the PWHT conditions and (b) EDS analysis showing the chemical composition data across the various locations in the fusion zone.

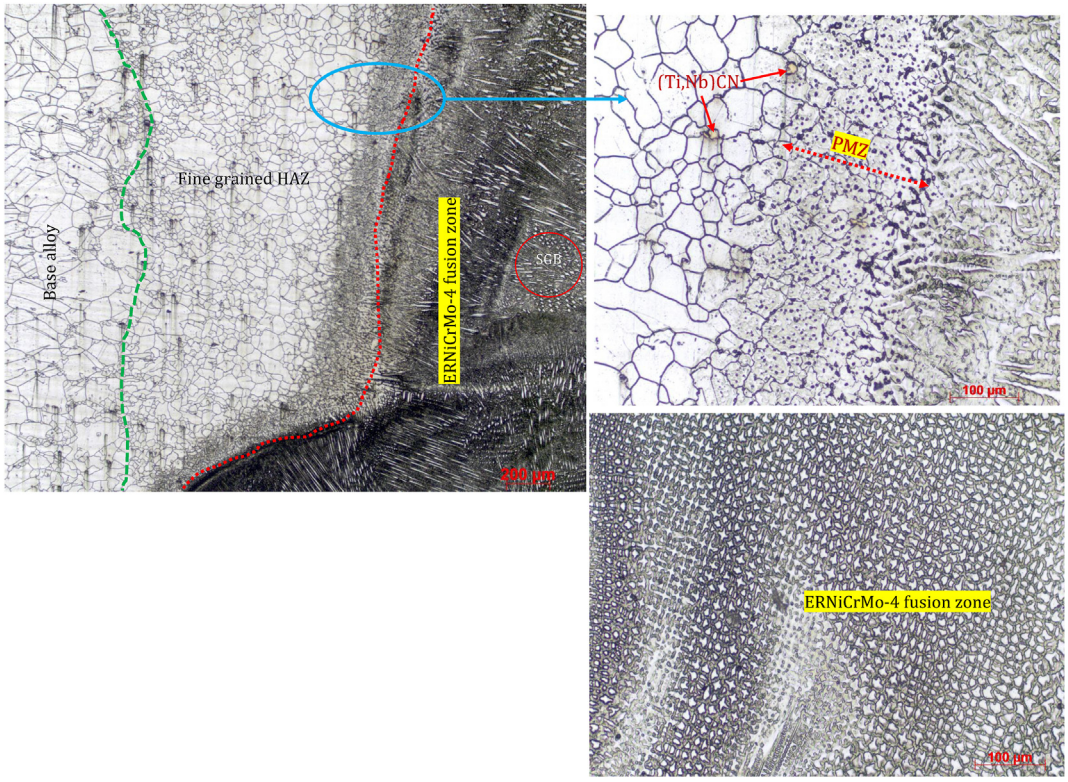

Fig. 6 – Optical micrographs show the formation of fine-grained HAZ in the PDCGTAW joints of Inconel 718 employing ERNiCrMo-4 in the as-welded conditions.

nucleation and thus favour the formation of solidification grain boundaries (SGBs) as indicated in Fig. 6. The equiaxed dendrites were observed predominantly in the centre of the FZ.

The discontinuous Nb-rich Laves phase and the Mo-Nb-rich precipitates are formed in the FZ of PDCGTAW joints as shown in Fig. 7 and further EDS analysis also confirmed the segregation of these phases. The EDS spectrum 1 of Fig. 7 indicated the zones with higher concentrations of Mo and Nb and the matrix is depleted of Nb. It is a fact that the precipitation of secondary phases becomes inevitable due to the partitioning of these elements. Also, the zones depleted with Mo make the FZ vulnerable to localized corrosion attack. Similar reports are found in the research work by Cortés et al. [14]. A higher concentration of Mo is observed in the FZ as Mo has a lower diffusivity than Nb. Also, as reported by Manikandan et al. [15] and Anbarasan et al. [16] a constitutional supercooling is much encouraged by the concentration gradient of Mo. According to these authors, the Mo-rich fillers result in grain refinement due to the pileup of solutes at the dendritic root which leads to the fragmentation of dendrites.

Upon multi-stage ageing, there are no substantial changes in the grain size of the HAZ as inferred from the optical microscopy analysis. The FE-SEM analysis shown in Fig. 8 revealed the occurrence of intragranular precipitation of thin plates δ-phase predominantly in the interdendritic regions of the PDCGTAW joints. The authors noticed an insignificant amount of γ″ phase in the fusion zone of the PDCGTA welds despite the double ageing at 720 °C/8 h and 620 °C/8 h which is reasoned to ERNiCrMo-4 filler, which lacks in Al and Ti. Due to the partitioning of Nb into the interdendritic regions upon solidification, the Nb-rich segregates are observed in Fig. 7. These Nb-rich segregates become the preferential sites for the precipitation of the δ-phase. As stated by Azadian et al. [17], the precipitation of the δ-phase occurs at the expense of the strengthening phase (γ″). The kinetics of the formation of the δ-phase was studied in detail by Dutta & Rettenmayr [18]. In the current study, the δ-phase precipitation occurs at 900 °C at the prior particle boundaries as well as the grain boundaries.

3.2. *Mechanical property assessment of the welds*

3.2.1. *Hardness measurements*

Followed by the metallurgical characterization of the weld joints, hardness measurements were carried out on the specimens extracted from the LAHW and PDCGTAW joints in both conditions. The hardness plots of these weld joints in both conditions are shown in Fig. 9 and the values are presented in Table 4. The base alloy experienced a substantial rise in hardness (≅120.01%) after subjecting to the solutionizing and double ageing treatments. The higher hardness imparted in the base alloy is due to solutionizing and double ageing heat treatments, which, in turn, resulted in the precipitation of the γ′ and γ″ strengthening phases as stated by Cortés et al. [14]. The hardness values at the HAZ of both joints are almost the same values as the base metal in the as-welded conditions. Upon solutionizing and double ageing, the hardness at the HAZ of

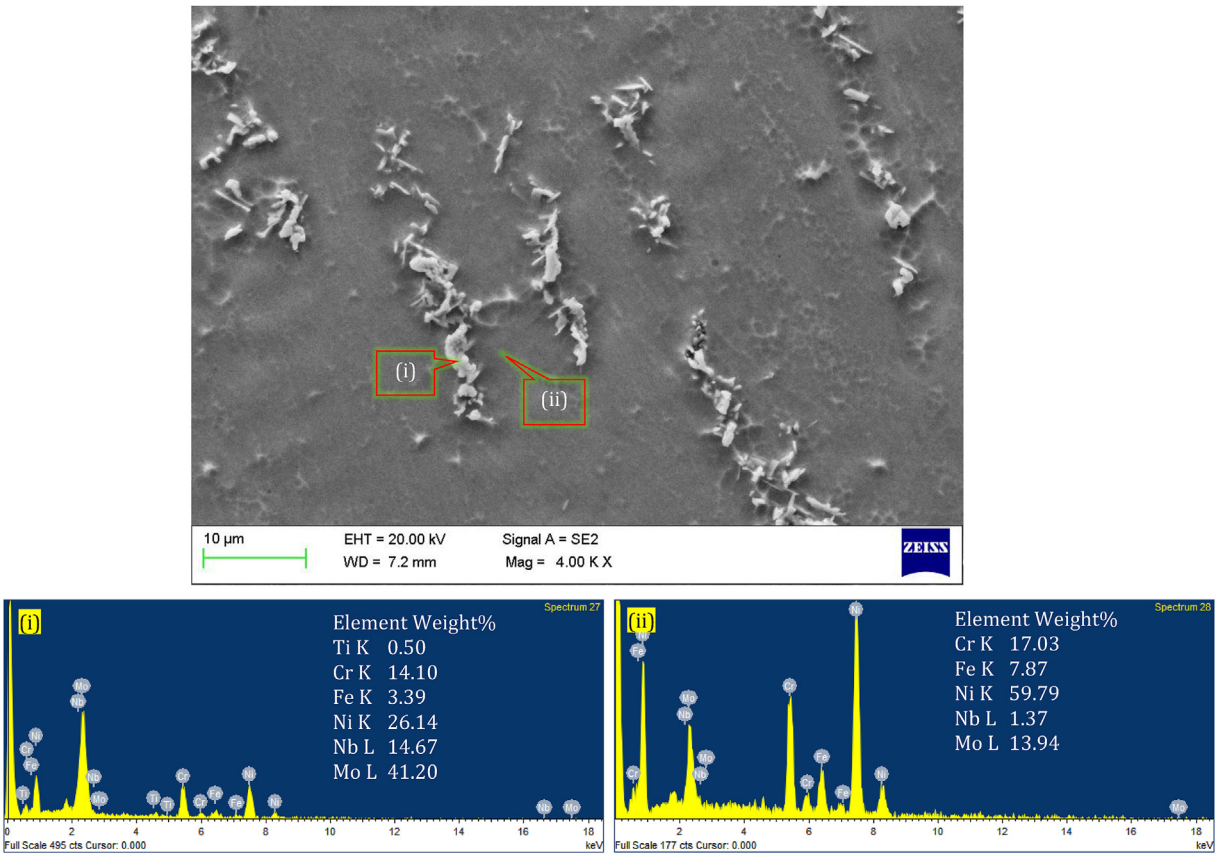

Fig. 7 – FE-SEM and EDS analysis at the fusion zone of Inconel 718 joints employing ERNiCrMo-4 in the as-welded conditions.

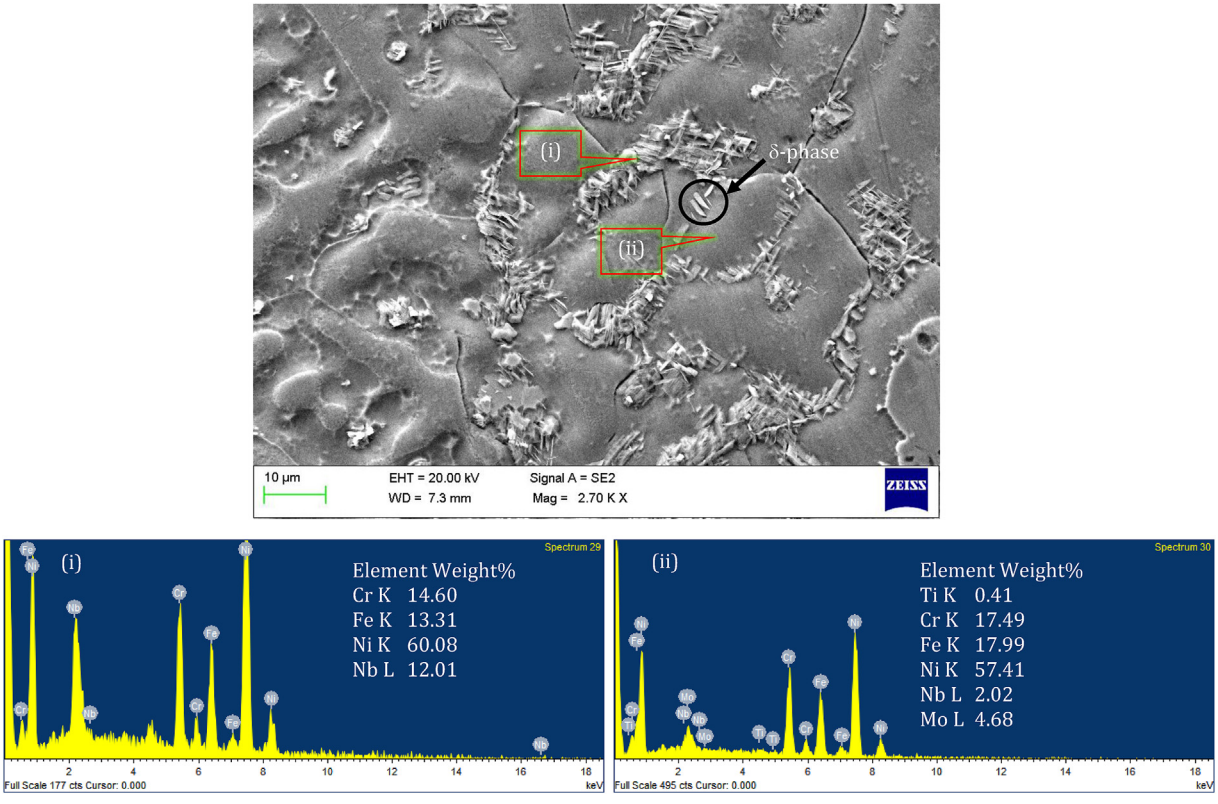

Fig. 8 – FESEM/EDS analysis on the PDCGTA weld joints of Inconel 718 indicating the formation of δ-Ni3Nb needles in the PWHT conditions.

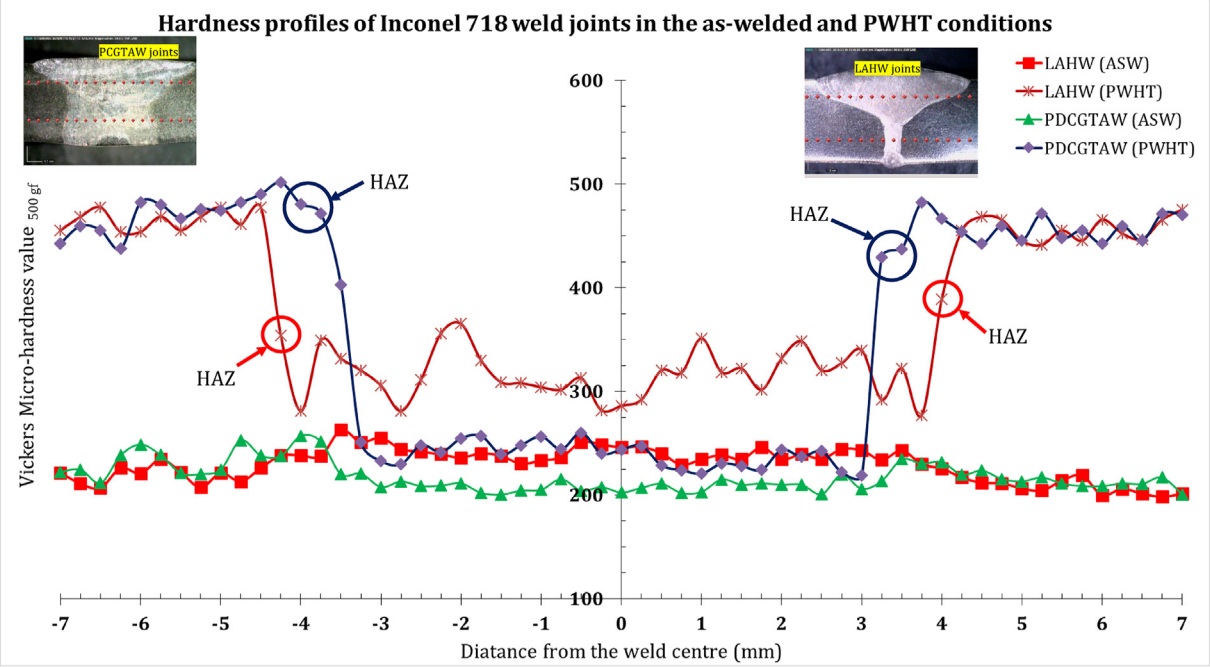

Fig. 9 – Vickers' micro-hardness profiles of Inconel 718 weld joints in the as-welded and PWHT conditions.

Table 4 – Vickers micro-hardness data of Inconel 718 base alloy and weld joints.

Vickers micro-hardness value (HV $_{500gf}$)					
Base Alloy		LAHW joints		PDCGTAW joints	
As-received	Aged	As-welded	PWHT	As-welded	PWHT
209 ± 7	460 ± 8.0	240 ± 7.0	319 ± 11.0	209 ± 6.0	239 ± 11.0

both joints increased considerably compared to the fusion zones. The potential reason for the rise in hardness values is associated with the grain boundary carbides, which is consistent with the microstructure studies, On the other hand, the PDCGTA welds experienced a lower hardness than the LAHW joints even after subjecting the joints to the PWHT conditions. The average hardness reported by the PCGTAW and LAHW joints is found to be 209 ± 6.0 and 240 ± 7.0 HV respectively in the as-welded conditions. The PDCGTAW joints experienced an increase in hardness to 14.35%; whereas the LAHW joints showed a rise in hardness to 32.92% after subjecting to PWHT conditions. The lower hardness in the FZ of both joints is attributed to the Nb-free filler wire employed in the study which experienced a sluggish response to the ageing. The scattering or impoverishing trend of hardness values in the FZs against the base metal is associated with the phenomena of convection experienced in the weld region along with the variation in the supersaturation of strengthening elements Nb and Mo in the γ-matrix as stated by Ramkumar et al. [19].

3.2.2. *Tensile properties of welds*

The results of the tensile studies are well in accordance with the hardness data. It is opined from the studies that amidst the HAZ liquation cracking was noticed, the LAHW joints experienced greater tensile and yield strengths in the PWHT conditions as shown in Table 5. The base metal Inconel 718

Table 5 – Tensile properties of the base alloys and weld joints.

Mechanical Property	Unit		Base Metal		PDCGTAW joints		LAHW joints	
			As-received	Solutionized and Aged	As-welded	Solutionized and Aged	As-welded	Solutionized and Aged
Yield strength	MPa	:	917.0	1115	425	480	489	985
Ultimate tensile strength	MPa	:	992.5	1310	796	820	798	1170
% elongation	%	:	27.75	28.5	20.75	13.5	45	8.25
Fracture Location	–	:	–	–	Weld	Weld	Weld	Weld
Joint Efficiency	%	:	–	–	80.2	62.5	80.8	89.3

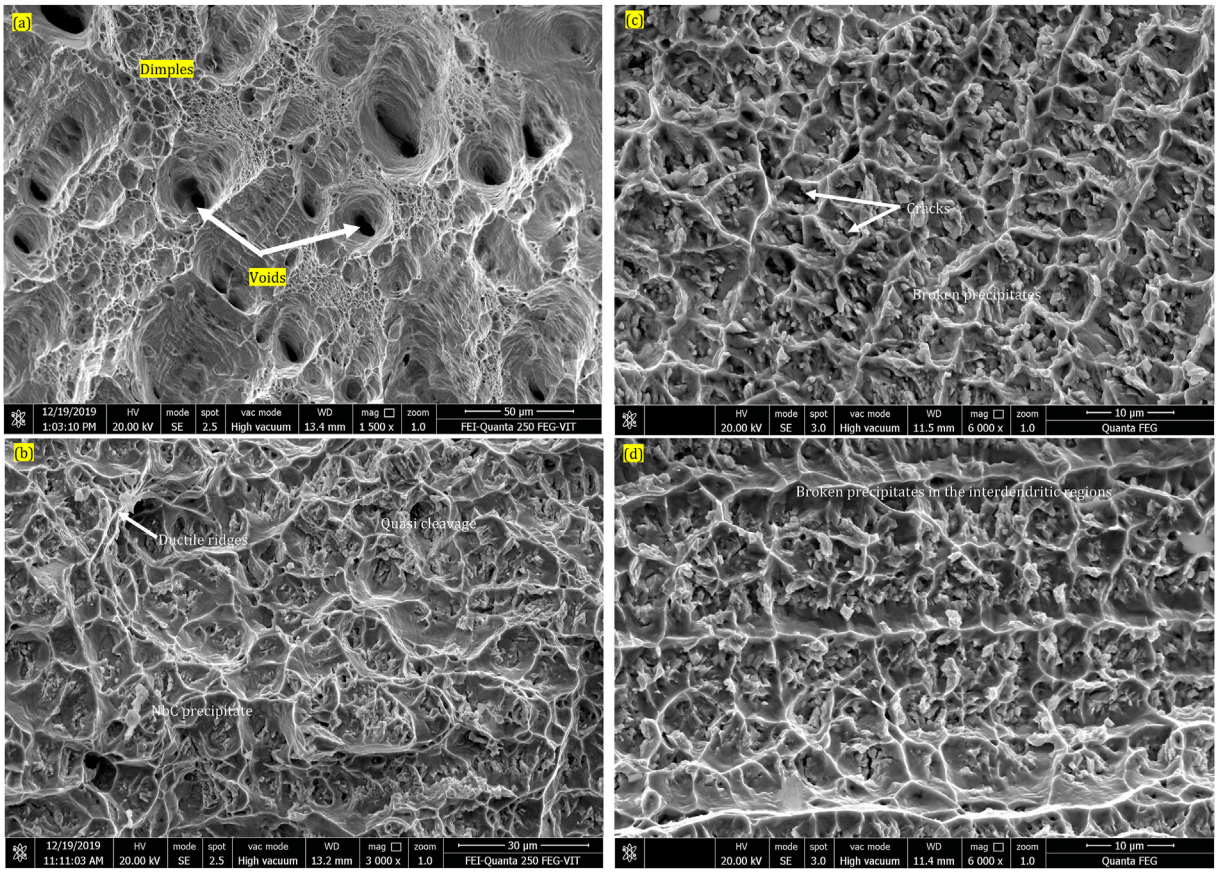

Fig. 10 – FE-SEM images showing the fractographic traits of the tensile ruptured Inconel 718 (a) and (b) PDCGTAW joints and (c) and (d) LAHW joints in the as-welded and PWHT conditions.

experienced an outstanding improvement in tensile strength after subjecting to solutionized and double-aged conditions which is attributed to the precipitation of γ' and γ'' strengthening phases. Upon tensile loading, the dislocations require more load to bypass or cut the hardening γ' precipitates in addition to the strain imposed by the γ'' phase in γ-FCC matrix. As pointed out by DuPont [20], the γ'' phase whose crystal structure is BCT is coherent γ-FCC matrix. Also, the author stated that the strain developed due to the mismatch in the lattice between γ and γ' increases the mechanical properties of Inconel 718 at room and low temperatures.

On the contrary, the tensile studies opined that both the LAHW and PDCGTAW joints experienced tensile fractures in the FZ in both conditions. A marginal rise in the tensile strengths of 3.02% and 46.61% for PDCGTAW and LAHW joints respectively was observed after subjecting to PWHT conditions. The tensile results also indicated that the LAHW joints experienced a greater yield strength in comparison to that of PDCGTAW joints in the solutionised and aged conditions. The percentage elongation of both joints was impoverished compared to that of the base metal in the solutionized and aged conditions. This is reasoned to the formation of coarse MC-carbides and the δ-phase in the fusion zone of both joints after subjecting to double ageing treatments. The voids coalesced in the dimpled facets observed in Fig. 10(a) of the PDCGTAW joints in the as-welded conditions indicated a ductile fracture mode. Whereas, a quasi-cleavage fracture is noticed on the same joints after being exposed to solutionized and aged conditions [Fig. 10(b)]. On the contrary, the LAHW joints experienced quasi-cleavage failure in both as-welded and aged conditions showing the appearance of a dendritic pattern. The evolution of Nb-Mo-rich segregates in the interdendritic regions and also the carbides corroborated the brittle fracture. The segregated particles served as the favourable sites for initiating the microvoids and offer the fracturing easier by the growth of macroscopic voids along the interfaces of Nb-segregates/matrix resulting in lower tensile percent elongation.

4. Conclusions

The findings based on the process specifications adopted in the current studies are as follows.

[1] Laser-arc hybrid welding and pulsating direct current GTA welding techniques were adopted successfully to join the Inconel 718 plates using Nb-free filler.
[2] Liquation cracking was noticed in the heat-affected zone of the LAHW joints due to the evolution of MC-type carbides.
[3] The dissolution of Nb-Mo rich phases, the evolution of strengthening phases γ' and γ'' and MC were noticed as

the microstructural traits after subjecting to solutionizing and ageing.

[4] Discontinuous Nb-rich Laves phase and Mo-rich segregates were noticed in the FZ of PDCGTAW joints in the as-welded condition and the δ-phase emanated due to the dissolution of Nb in the aged conditions.

[5] The tensile properties of the LAHW joints were increased considerably after subjecting to the solutionizing and double ageing treatments.

[6] Tensile failures were observed in the weld region of both the joints in both the as-welded and aged conditions. The joint efficiencies achieved by the LAHW and PDCGTAW joints are 62.5% and 89.3% in the solutionized and double-aged conditions.

Data availability statement

All the raw and processed data are provided in the manuscript itself. Additional data if any, will be provided based on the request.

Declaration of interests

The authors declare that they have no known competing financial interests or personal relationships that could have appeared to influence the work reported in this paper.

Acknowledgement

The authors express their thankfulness to the Royal Academy of Engineering, United Kingdom for the funding provided as a part of the Distinguished International Associates (DIA) [DIA-2021-144]. The authors wish to acknowledge VIT Vellore for providing the SEM and EDS facilities for our research work.

REFERENCES

[1] Niang A, Huez J, Lacaze J, Viguier B. Characterizing precipitation defects in nickel based 718 alloy. Materials Science Forum 2010;636–637:517–22. Trans Tech Publications Ltd, https://doi.org/10.4028/www.scientific.net/MSF.636-637.517.

[2] Radhakrishna CH, Rao KP. The formation and control of Laves phase in superalloy 718 welds. vol. 32; 1997.

[3] Dev S, Ramkumar KD, Arivazhagan N, Rajendran R. Effect of continuous and pulsed current GTA welding on the performance of dissimilar welds involving aerospace grade alloys. Trans Indian Inst Metal 2017;70(3):729–39. https://doi.org/10.1007/s12666-017-1085-y.

[4] Hong JK, Park JH, Park NK, Eom IS, Kim MB, Kang CY. Microstructures and mechanical properties of Inconel 718 welds by CO2 laser welding. J Mater Process Technol 2008;201:515–20. https://doi.org/10.1016/j.jmatprotec.2007.11.224.

[5] Janaki Ram GD, Venugopal Reddy A, Prasad Rao K, Reddy GM, Sarin Sundar JK. Microstructure and tensile properties of Inconel 718 pulsed Nd-YAG laser welds. J Mater Process Technol 2005;167:73–82.

[6] Appa Rao G, Srinivas M, Sarma DS. Effect of solution treatment temperature on microstructure and mechanical properties of hot isostatically pressed superalloy Inconel* 718. Mater Sci Technol 2004;20(9):1161–70. https://doi.org/10.1179/026708304225022124.

[7] Bang HS, Bang HS, Kim YC, Oh IH. A study on mechanical and microstructure characteristics of the STS304L butt joints using hybrid CO2 laser-gas metal arc welding. Mater Des 2011;32(4):2328–33. https://doi.org/10.1016/j.matdes.2010.12.039.

[8] Liu T, Yan F, Liu S, Li R, Wang C, Hu X. Microstructure and mechanical properties of laser-arc hybrid welding joint of GH909 alloy. Opt Laser Technol 2016;80:56–66. https://doi.org/10.1016/j.optlastec.2015.12.020.

[9] Liu W, Ma J, Atabaki MM, Pillai R, Kumar B, Vasudevan U, et al. Hybrid laser-arc welding of 17-4 PH martensitic stainless steel. Laser Manuf Mater Process 2015;2(2):74–90. https://doi.org/10.1007/s40516-015-0007-2.

[10] Muhammad S, Miikka K, Suck-Joo N, Sang-Woo H, Veli K. Effect of leading and trailing torch configuration on mixing and fluid behavior of laser-gas metal arc hybrid welding. J Laser Appl 2017;29(4):042009. https://doi.org/10.2351/1.5008304.

[11] Radavich JF. A high-temperature study of phase precipitation in superalloys. Adv X-Ray Anal 1959;3:365–75. https://doi.org/10.1154/S0376030800000926.

[12] Yan F, Liu S, Hu C, Wang C, Hu X. Liquation cracking behavior and control in the heat affected zone of GH909 alloy during Nd:YAG laser welding. J Mater Process Technol 2017;244:44–50. https://doi.org/10.1016/j.jmatprotec.2017.01.018.

[13] An XL, Zhou L, Zhang B, J J, Chu CL, Han LY, et al. Inconel 718 treated with two-stage solution and aging processes: microstructure evolution and enhanced properties. Mater Res Express 2019;6(7):075803. https://doi.org/10.1088/2053-1591/ab1290.

[14] Cortés R, Barragán ER, López VH, Ambriz RR, Jaramillo D. Mechanical properties of Inconel 718 welds performed by gas tungsten arc welding. Int J Adv Manuf Technol 2018;94(9–12):3949–61. https://doi.org/10.1007/s00170-017-1128-x.

[15] Manikandan SGK, Sivakumar D, Rao KP, Kamaraj M. Effect of weld cooling rate on Laves phase formation in Inconel 718 fusion zone. J Mater Process Technol 2014;214(2):358–64. https://doi.org/10.1016/j.jmatprotec.2013.09.006.

[16] Anbarasan N, Jerome S, Manikandan SGK. Hydrogen and molybdenum control on laves phase formation and tensile properties of inconel 718 GTA welds. Mater Sci Eng A 2020;773. https://doi.org/10.1016/j.msea.2019.138874.

[17] Azadian S, Wei LY, Warren R. Delta phase precipitation in inconel 718. Mater Character 2004;53(1):7–16. https://doi.org/10.1016/j.matchar.2004.07.004.

[18] Dutta B, Rettenmayr M. An experimental investigation on the kinetics of solute driven remelting. Metall Mater Trans A 2000;31(11):2713–20. https://doi.org/10.1007/BF02830330.

[19] Ramkumar KD, Mulimani SS, Ankit K, Kothari A, Ganguly S. Effect of grain boundary precipitation on the mechanical integrity of EBW joints of Inconel 625. Mater Sci Eng, A 2021;808:140926. https://doi.org/10.1016/j.msea.2021.140926.

[20] DuPont JN. A combined solubility product/new PHACOMP approach for estimating temperatures of secondary solidification reactions in superalloy weld metals containing Nb and C. Metall Mater Trans A 1998;29(5):1449–56. https://doi.org/10.1007/s11661-998-0360-2.

FURTHER READING

22 Ramkumar KD, Dharmik K, Noronha B, Giri Mugundan K, Bhargav S, Phani Prabhakar KV. Structure-property evaluation of single pass Laser-arc hybrid welding of re-sulphurized martensitic stainless steel. J Mater Process Technol 2019;271:413–9. https://doi.org/10.1016/j.jmatprotec.2019.04.016.

2023-09-07

Effect of solutionizing and double ageing treatments on the microstructural characteristics and tensile properties of Inconel 718 welds

Devendranath Ramkumar, K.

Elsevier

Ramkumar KD, Arvind AV, Aravinth KR, et al., (2023) Effect of solutionizing and double ageing treatments on the microstructural characteristics and tensile properties of Inconel 718 welds, Journal of Materials Research and Technology, Volume 26, September-October 2023, pp. 6255-6265
https://doi.org/10.1016/j.jmrt.2023.09.016